Zhang et al. *Zool. Res.* 2024, 45(3): 468−477
https://doi.org/10.24272/j.issn.2095-8137.2023.385

ZR | Zoological Research

Article Open Access

Mitochondrial targeting sequence of magnetoreceptor MagR: More than just targeting

Yanqi Zhang[1,2], Peng Zhang[1,2], Junjun Wang[1], Jing Zhang[1,2], Tianyang Tong[1,3], Xiujuan Zhou[1,2], Yajie Zhou[1,4], Mengke Wei[1,4], Chuanlin Feng[1,2], Jinqian Li[5], Xin Zhang[1,2,4,6], Can Xie[1,2,6,7,*], Tiantian Cai[1,2,7,*]

[1] *High Magnetic Field Laboratory*, *Hefei Institutes of Physical Science*, *Chinese Academy of Sciences*, *Hefei*, *Anhui* 230031, *China*
[2] *University of Science and Technology of China*, *Hefei*, *Anhui* 230026, *China*
[3] *Department of Anatomy*, *School of Basic Medicine*, *Anhui Medical University*, *Hefei*, *Anhui* 230032, *China*
[4] *Institutes of Physical Science and Information Technology*, *Anhui University*, *Hefei*, *Anhui* 230039, *China*
[5] *Key Laboratory of Tropical Translational Medicine of Ministry of Education*, *NHC Key Laboratory of Tropical Disease Control*, *School of Tropical Medicine and The Second Affiliated Hospital*, *Hainan Medical University*, *Haikou*, *Hainan* 571199, *China*
[6] *International Magnetobiology Frontier Research Center*, *Science Island*, *Hefei*, *Anhui* 230031, *China*
[7] *Institute of Quantum Sensing*, *Zhejiang University*, *Hangzhou*, *Zhejiang* 310027, *China*

ABSTRACT

Iron-sulfur clusters are essential cofactors for proteins involved in various biological processes, such as electron transport, biosynthetic reactions, DNA repair, and gene expression regulation. Iron-sulfur cluster assembly protein IscA1 (or MagR) is found within the mitochondria of most eukaryotes. Magnetoreceptor (MagR) is a highly conserved A-type iron and iron-sulfur cluster-binding protein, characterized by two distinct types of iron-sulfur clusters, [2Fe-2S] and [3Fe-4S], each conferring unique magnetic properties. MagR forms a rod-like polymer structure in complex with photoreceptive cryptochrome (Cry) and serves as a putative magnetoreceptor for retrieving geomagnetic information in animal navigation. Although the N-terminal sequences of MagR vary among species, their specific function remains unknown. In the present study, we found that the N-terminal sequences of pigeon MagR, previously thought to serve as a mitochondrial targeting signal (MTS), were not cleaved following mitochondrial entry but instead modulated the efficiency with which iron-sulfur clusters and irons are bound. Moreover, the N-terminal region of MagR was required for the formation of a stable MagR/Cry complex. Thus, the N-terminal sequences in pigeon MagR fulfil more important functional roles than just mitochondrial targeting. These results further extend our understanding of the function of MagR and provide new insights into the origin of magnetoreception from an evolutionary perspective.

Keywords: Magnetoreceptor (MagR); N-terminal sequence; Mitochondrial targeting signal; Iron-sulfur cluster

INTRODUCTION

Iron-sulfur cluster-binding proteins constitute one of the most ancient classes of metalloproteins in nature, present in all living organisms and playing vital roles in diverse biological processes, including electron transport, metabolism, biosynthetic reactions, DNA repair, and gene expression regulation. Three iron-sulfur cluster biogenesis machineries, including iron-sulfur cluster (ISC), sulfur utilizing factor (SUF), and nitrogen fixation (NIF) systems, have been identified across both prokaryotes and eukaryotes (Garcia et al., 2022; Tsaousis, 2019).

The ISC machinery is recognized as a housekeeping system for cellular maintenance, primarily localized within the mitochondria of eukaryotes, although it has also been detected in the cytoplasm and nucleus in some eukaryotes, including humans (Song et al., 2009). Maintaining ISC assembly is suggested to underpin the existence of mitochondria (Hjort et al., 2010; Lill et al., 1999), fundamental for the evolution of eukaryotes. IscA, a key component of the ISC machinery, is widely distributed across biological

Received: 13 December 2023; Accepted: 25 January 2024; Online: 26 January 2024

Foundation items: This study was supported by the National Natural Science Foundation of China (31640001 and T2350005 to C.X., U21A20148 to X.Z. and C.X.), Ministry of Science and Technology of China (2021ZD0140300 to C.X.), Natural Science Foundation of Hainan Province (No. 822RC703 for J.L.), Foundation of Hainan Educational Committee (No. Hnky2022-27 for J.L.), and Presidential Foundation of Hefei Institutes of Physical Science, Chinese Academy of Sciences (Y96XC11131, E26CCG27, and E26CCD15 to C.X., E36CWGBR24B and E36CZG14132 to T.C.)

*Corresponding authors, E-mail: canxie@zju.edu.cn; tiantiancai@pku.edu.cn

kingdoms, from bacteria to mammals, underscoring its evolutionary significance. In *Escherichia coli*, IscA is encoded by the *isc* operon, while in most eukaryotes, from yeast to humans, two A-type proteins, IscA1 (yeast Isa1) and IscA2 (yeast Isa2), are encoded by nuclear genes and predominantly localized in the mitochondria (Beilschmidt et al., 2017).

IscA in prokaryotes and IscA1 and IscA2 in eukaryotes are crucial for binding iron and iron-sulfur clusters and serve as iron donors, particularly during iron-sulfur cluster assembly, or as iron-sulfur carrier/scaffold proteins that provide iron-sulfur clusters to acceptor proteins. IscA1 and IscA2 also play essential roles in the maturation of mitochondrial [4Fe-4S] proteins, with different IscA isoforms fulfilling different roles (Beilschmidt et al., 2017). IscA1 has attracted increasing attention due to its potential role as a putative magnetoreceptor (MagR), contributing to magnetic sensing (or magnetoreception) and navigation capabilities in animals.

While magnetoreception has evolved in various migratory and homing species, the underlying mechanism remains poorly understood. Various theoretical models have been proposed to explain this phenomenon, including the magnetite-based model (Eder et al., 2012; Hsu et al., 2011; Monteil & Lefevre, 2020; Walcott et al., 1979), cryptochrome (Cry)-based radical-pair model (Gegear et al., 2008; Hore & Mouritsen, 2016; Schulten & Wolynes, 1978; Xu et al., 2021), and MagR/Cry biocompass model (Qin et al., 2016; Xie, 2022). In the biocompass model, MagR, originally known as IscA1, interacts with Cry to create a rod-like structure measuring 15×24 nm that exhibits an intrinsic magnetic moment. This enables the sensing of both polarity and inclination of the geomagnetic field in a manner influenced by light and magnetic fields (Qin et al., 2016; Xie, 2022). Recent findings have unveiled the functional roles of the MagR/Cry complex, including the identification of two distinct iron-sulfur clusters, [2Fe-2S] and [3Fe-4S], each conferring unique magnetic properties (Guo et al., 2021), and the discovery of a separate mononuclear iron binding site in pigeon (*Columba livia*) MagR (clMagR), where iron and iron-sulfur binding collectively enhance protein magnetism (Zhou et al., 2023). Tetramers serve as the building block of MagR polymers, and the external magnetic field can induce MagR assembly *in vitro* (Arai et al., 2022, 2023; Yang et al., 2022). Interestingly, MagR expression exhibits daily oscillations and is significantly higher in certain migratory species (Chang et al., 2017, 2018; Jin et al., 2023; Mannino et al., 2023). A recent study demonstrated that MagR knockdown in oriental armyworms (*Mythimna separata*) *in vivo* abolished their magnetic orientation, underscoring the vital role of MagR in magnetic sensing at the physiological level (Tong et al., 2022a).

Despite significant progress in understanding the functions and magnetism of MagR, much remains to be answered. For example, while the C-terminal region of MagR is highly conserved, the N-terminal sequences exhibit considerable variability across species, and their specific role in MagR remains incompletely defined. It has been proposed that the N-terminal sequences of MagR may play a role in concatenating two neighboring MagR tetramers within the magnetoreceptor polymer and participate in the formation of the biocompass complex, as evidenced by molecular dynamics simulations (Lu et al., 2020). However, this hypothesis requires additional experimental validation.

This study revealed that the first 25 amino acids at the N-terminal of pigeon MagR acted as a mitochondrial targeting signal and were not cleaved after protein maturation, as confirmed by cellular assays. Moreover, the 25 amino acids affected the binding efficiency but not the type of iron-sulfur clusters. Notably, MagR/Cry complex formation required the involvement of the N-terminal sequences. The findings presented in this study expand our understanding of the specific and critical functions of the N-terminal sequences of MagR, offering valuable insights into magnetoreception and its evolutionary trajectory across species.

MATERIALS AND METHODS

Plasmid construction

The DNA sequences for the full-length pigeon (*Columba livia*) MagR (clMagR) were synthesized by Sangon Biotech (China). In the cell-based assays, constructs of full-length clMagR ($clMagR^{WT}$) and clMagR with the N-terminal 25 residues deleted ($clMagR^{\Delta N25}$), each tagged with Flag-tag or EGFP at the C-terminal, along with constructs featuring EGFP alone or EGFP fused with the N-terminal 25 residues of clMagR, were cloned into the pcDNA 3.1 hygro (-) vector for mammalian expression. For bacterial expression, DNA sequences encoding wild-type clMagR ($clMagR^{WT}$), clMagR with the N-terminal 25 residues deleted ($clMagR^{\Delta N25}$), IscA from *E. coli* with a Strep-tag II at the N-terminal, and wild-type clCry4 ($clCry4^{WT}$) with a His-tag fused at the N-terminal were cloned into the pCold vector, as described previously (Qin et al., 2016). All constructs were verified by Sanger sequencing.

Cell culture

HeLa cells were maintained in Dulbecco's Modified Eagle's Medium (DMEM, Corning, USA) containing 10% fetal bovine serum, 2 mmol/L GlutaMAX, and 1% penicillin/streptomycin and incubated at 37°C in a humidified incubator (Thermo Fisher Scientific, USA) with 5% CO_2. Fresh culture medium was substituted every 1 to 2 days.

Transfection of HeLa cells

HeLa cells were seeded on coverslips in 6-well-plates and cultivated until reaching 50% confluence. For each well, 2 μg of plasmid was transfected according to the guidelines provided by the manufacturers of Lipofectamine™ 3000 Reagent (Invitrogen, USA). After 24 h of incubation at 37°C, the cells were washed with phosphate-buffered saline (PBS) for immunofluorescence staining or harvested for western blotting.

Western blotting

Cells were washed once with PBS before being detached from the culture plates with a cell scraper and lysed in M-PER™ Mammalian Protein Extraction Reagent (Thermo Fisher Scientific, USA) in the presence of protease inhibitors (Sigma, USA). The lysates were then centrifuged at 12 000 ×*g* for 20 min at 4°C. The supernatants were transferred to clean tubes and added with loading buffer (50 mmol/L Tris-HCl pH 6.8, 2% sodium dodecyl-sulfate (SDS), 10% glycerol, 12.5 mmol/L ethylenediaminetetraacetic acid (EDTA), 0.02% bromophenol blue, 50 mmol/L dithiothreitol (DTT)). After incubation at 95°C for 5 min, the protein samples were loaded on 15% polyacrylamide gel. After gel electrophoresis, proteins were transferred to polyvinylidene fluoride membranes, blocked with 5% skimmed milk (in TBS-Tween buffer) for 1 h, and incubated overnight at 4°C with primary antibodies: mouse anti-Flag (1:2 000, Sigma-Aldrich, USA) and mouse anti-

GAPDH (1:1 000, TransGen Biotech, China). The membranes were washed three times with fresh TBS-Tween buffer and incubated with horseradish peroxidase (HRP)-labeled secondary antibody against mouse IgG (1:3 500, Cell Signaling Technology, USA). The membranes were washed three times with TBS-Tween buffer and the HRP signal was detected using an Immobilon Western HRP Substrate (Sigma Aldrich, USA).

Cell imaging

At 24 h post-transfection, cells were washed three times with PBS and fixed on coverslips with 4% paraformaldehyde solution for 30 min, followed by incubation with blocking buffer (0.2% sodium azide, 2% bovine serum albumin, and 0.1% Triton X-100 in TBS-Tween) for 30 min. The cells were then incubated with primary antibodies overnight at 4°C in a humid chamber. The primary antibodies included: anti-Flag(R) M2 antibody (1:1 000, Sigma Aldrich, USA) and Tom20 Rabbit mAb (1:500, Cell Signaling Technology, USA). After incubation, the coverslips were washed once with TBS-Tween buffer and incubated with Alexa Fluor™ 488 (Thermo Fisher Scientific, USA) or Alexa Fluor 594-conjugated secondary antibodies (Cell Signaling Technology, USA) for 1 h at room temperature. All coverslips were stained with 4',6-diamidino-2-phenylindole (DAPI, 1 μg/mL) for 5 min and washed three times with PBS. Finally, the coverslips were mounted in antifade mounting medium (Beyotime, China) before imaging. All immunofluorescence images were captured using a confocal microscope (Olympus SpinSR10, Japan). Average fluorescence intensity of Tom20 was quantified with ImageJ and the data were plotted using GraphPad Prism.

Protein expression and purification

The expression constructs of clMagR were generated as described previously (Qin et al., 2016). The clMagR^{WT}, clMagR$^{\Delta N25}$, and IscA from *E. coli* and wild-type clCry4 genes were cloned into pCold vector and transformed into the *E. coli* strain BL21 (DE3). Cultures were incubated at 37°C and 220 r/min until OD600 reached 0.6. Protein expression was induced with 20 mmol/L IPTG overnight (~20 h) at 15°C. Cells were harvested by centrifugation for 30 min at 8 000 ×*g* and 4°C and resuspended in lysis buffer (20 mmol/L Tris, 500 mmol/L NaCl, pH 8.0) and lysed by sonication on ice. Cell debris was removed by centrifugation at 17 500 ×*g* for 45 min at 4°C. For clMagR and IscA purification, the supernatants were loaded onto a Strep-Tactin affinity column (IBA GmbH, Germany). After washing with 20 column volumes (CV) of washing buffer (20 mmol/L Tris, 150 mmol/L NaCl, pH 8.0) to remove unbound proteins, proteins were eluted using elution buffer (20 mmol/L Tris, 150 mmol/L NaCl, 5 mmol/L desthiobiotin, pH 8.0).

For the purification of the clMagR/clCry4 complex, clCry4 fused with His-tag and full-length clMagR or clMagR$^{\Delta N25}$ fused with Strep-tag II at the N-terminal were co-expressed in *E. coli* BL21 (DE3) at 15°C, then induced by 20 mmol/L IPTG. For each co-expression, clCry4 with wild-type or truncated clMagR, the soluble fraction of *E. coli* lysis was first loaded onto a Ni-NTA matrix (Qiagen, Germany). After using washing buffer (20 mmol/L Tris, 150 mmol/L NaCl, 20 mmol/L imidazole, pH 8.0), the proteins were eluted from the Ni-NTA matrix using elution buffer (20 mmol/L Tris, 150 mmol/L NaCl, 300 mmol/L Imidazole, pH 8.0). The complex proteins were then further purified by direct application to a Strep-Tactin column (IBA GmbH, Germany) and eluted using IBA elution buffer (20 mmol/L Tris, 150 mmol/L NaCl, 5 mmol/L desthiobiotin, pH 8.0). The complex products were checked with sodium dodecyl-sulfate polyacrylamide gel electrophoresis (SDS-PAGE). All samples were supplemented with standard sample loading buffer containing SDS and heated at 95°C for 5 min before loading for SDS-PAGE.

IscU and IscS were cloned into pCold vector with a His-tag fused on the N-terminal and expressed in the *E. coli* strain BL21 (DE3). Purification was performed using Ni-NTA affinity chromatography (Qiagen, Germany), as described above. The purity of all purified proteins was determined using SDS-PAGE. PageRuler Prestained Protein Ladder (Thermo Scientific, Product# 26616, USA) was used as the molecular weight standard.

Ferrozine assay

Ferrous iron reacts with ferrozine to form a stable purple complex that can be quantified spectrophotometrically at 562 nm (Im et al., 2013). Thus, total iron content can be determined by quantitatively reducing Fe^{3+} to Fe^{2+} using hydroxylamine-HCl (10% (w/v) HAHCl in 1 mol/L HCl) and monitoring absorbance at 562 nm. Here, a series of ferric chloride ($FeCl_3$) solutions (0.1–1.0 mmol/L) prepared in HCl (1 mol/L) were used to generate a standard curve. Subsequently, 20 μL of protein (0.1 mmol/L) and 80 μL of hydroxylamine-HCl (10% w/v HAHCl in 1 mol/L HCl) were added to each well of a microplate and incubated at room temperature in the dark for 30 min, after which 100 μL of ferrozine was added to each well and incubated at 37°C for an additional 15 min in the dark. Finally, the absorbances of these Fe^{2+}-ferrozine complexes were measured at 562 nm on a microplate reader (Tecan Spark, Switzerland). Iron levels in protein samples were determined by linear regression analysis. Three replicates for each protein sample were performed. Statistical significance was calculated using GraphPad Prism (two-tailed Student's *t*-test). Where relevant, statistical test results are indicated in the corresponding figures. **: $P<0.01$; ***: $P<0.001$.

Electronic paramagnetic resonance spectroscopy (EPR) measurement

X-band EPR spectra were recorded at various temperatures (10 K, 25 K, 45 K, and 60 K) using an EMX plus 10/12 Spectrometer (Bruker, Germany) equipped with an Oxford ESR910 Liquid Helium cryostat. The oxidized EPR samples were prepared by mixing 200 μL of 1 mmol/L purified protein with 50 μL of glycerol, while the reduced samples were obtained by adding sodium dithionite to a final concentration of 10 mmol/L to the above protein solutions. The protein samples were transferred to quartz EPR tubes (Wilmad 707-SQ-250 M, France) and frozen in liquid nitrogen. The EPR signals were collected at a microwave frequency of 9.40 GHz, microwave power of 2 mW, modulation amplitude of 2.0 G, receive gain of 1.0×10^4, and sweep time of 25.60 s.

Ultraviolet (UV)-visible absorption and analytical size-exclusion chromatography (SEC)

UV-visible absorption spectra (300–600 nm) were recorded for 200 μmol/L purified proteins at room temperature with a NanoDrop Spectrophotometer (Thermo Scientific, NanoDrop OneC, USA).

SEC was used to identify protein assembly states. Protein samples were centrifuged at 12 000 r/min for 10 min and the supernatant was loaded on a Superose 6 Increase 10/300 chromatography column equilibrated with TBS buffer

(20 mmol/L Tris, 150 mmol/L NaCl, pH 8.0).

Circular dichroism (CD) spectroscopy

CD spectroscopy was used to detect the secondary structures of the proteins in the far UV range (190–260 nm) and identify protein-bound cofactors such as iron-sulfur clusters. To analyze the type of iron-sulfur clusters, 100 μmol/L purified proteins were prepared and measured in the near UV-visible range (300–600 nm) at room temperature using a MOS-500 (Biologic, France) CD Spectrometer. To analyze the secondary structure of proteins, 10 μmol/L purified clMagR^{WT}, clMagR$^{\Delta N25}$, and IscA were prepared separately in 20 mmol/L sodium phosphate buffer and measured using a J-1700 CD Spectrometer (JASCO Corporation, Japan) in 1 mmol/L quartz cuvettes. Data were analyzed using Bestsel (BeStSel-Protein Circular Dichroism Spectra Analysis) and shown with the ellipticity value in mDeg.

Iron reconstitution in clMagR^{WT} and clMagR$^{\Delta N25}$

Purified clMagR^{WT} and clMagR$^{\Delta N25}$ (200 μmol/L) were separately incubated with $Fe(NH_4)_2(SO_4)_2$ (0–140 μmol/L) in the presence of 2 mmol/L DTT at room temperature for 5 min. After the reaction, proteins were purified using a PD MiniTrap G-25 desalting column (GE Healthcare, USA). Absorption peaks of the protein samples at 315 nm were used to determine relative iron binding in clMagR.

Chemical reconstitution of iron-sulfur clusters in IscU

Freshly purified IscU (apo-IscU) was mixed with 5 mmol/L DTT for 30 min at 4°C in buffer containing 20 mmol/L Tris, 150 mmol/L NaCl, and 5 mmol/L desthiobiotin (pH 8.0), followed by incubation with $Fe(NH_4)_2(SO_4)_2$ (1.6 mmol/L) and Na_2S (1.6 mmol/L) overnight at 4°C. Unbound iron and sulfide were removed via a PD MiniTrap G-25 desalting column (GE Healthcare, USA). The collected proteins were concentrated and labeled as “holo-IscU”. The iron-sulfur cluster assembly reactions were monitored with a UV-visible absorption spectrometer.

***In vitro* iron-sulfur cluster transfer**

Purified clMagR^{WT} or clMagR$^{\Delta N25}$ (400 μmol/L) in TBS buffer (20 mmol/L Tris, 150 mmol/L NaCl, pH 8.0) was incubated with 10 mmol/L $Na_2S_2O_4$ and 10 mmol/L EDTA overnight at 4°C to remove iron-sulfur clusters, followed by desalting through a PD MiniTrap G-25 desalting column (GE Healthcare, USA). The obtained protein samples were labeled as “apo-clMagR”. The holo-IscU was prepared following previous research (Beilschmidt et al., 2017; Zhou et al., 2023). Apo-clMagR was incubated with holo-IscU for approximately 3 h at 4°C in the presence of 5 mmol/L DTT. The two proteins were then separated using a Strep-Tactin affinity column (IBA GmbH, Germany) and their iron-sulfur cluster properties were monitored by UV-visible spectral analysis.

Iron transfer experiments

Previous studies have shown that iron-loaded IscA can provide iron for iron-sulfur cluster assembly in IscU *in vitro* under aerobic conditions (Ollagnier-de Choudens et al., 2003). For the iron transfer experiments, purified IscU (100 μmol/L) was incubated with clMagR (Strep-tagged, 150 μmol/L) and IscS (1 μmol/L) in buffer containing 2 mmol/L DTT, 1 mmol/L L-cysteine, 150 mmol/L NaCl, and 20 mmol/L Tris (pH 8.0) at 4°C for 3 h. After the reaction, the mixture was separated through affinity chromatography and UV-visible spectra were recorded to monitor iron transfer, as described above.

RESULTS

N-terminal 25 residues of clMagR are involved in mitochondrial localization

MagR and IscA are widely expressed in nearly all species and play fundamental roles in the biogenesis of iron-sulfur clusters. The sequences of MagR are highly conserved across species, particularly in the C-terminal region, as shown in the 10 representative species in Figure 1A. However, the first 25 amino acids of the N-terminal (here named N25) of MagR, as seen in the pigeon sequence, show considerable variation across species and are absent in *E. coli.* For example, the sequence similarity for full-length MagR between pigeons and humans was 94.7%, with the similarity in the C-terminal region reaching 100% but the N25 sequence similarity only showing 72%. Notably, the similarity between pigeon MagR and *E. coli* IscA was only 45.45% due to the absence of N25 sequences in *E. coli* IscA, highlighting the N-terminal sequence as a key distinguishing feature between eukaryotic MagR and prokaryotic IscA. Given the predominant mitochondrial localization of eukaryotic MagR proteins, we investigated whether the N25 play a role as a mitochondrial targeting signal, using the clMagR sequence from pigeons for subcellular localization testing. Full-length clMagR fused with a Flag-tag was highly expressed in HeLa cells, as confirmed by anti-Flag antibody imaging, and showed obvious colocalization with the mitochondrial outer membrane protein Tom20, indicating mitochondrial localization. However, when the N25 sequences of clMagR were truncated, clMagR$^{\Delta N25}$ was randomly distributed in the cytoplasm and nucleus, suggesting a loss of mitochondrial targeting ability (Figure 1B). Interestingly, expression of wild-type or N25-truncated clMagR fused with EGFP (clMagR^{WT}-EGFP and clMagR$^{\Delta N25}$-EGFP) in HeLa cells resulted in uniform cellular distribution, without obvious mitochondrial localization (Supplementary Figure S1A). This implies that larger tags such as EGFP (27 kDa), compared to the Flag-tag (1 kDa), may interfere with the correct subcellular localization of clMagR^{WT} (14 kDa) and clMagR$^{\Delta N25}$ (12 kDa), mirroring earlier findings showing fusion proteins tagged with large EGFP exhibited improper targeting compared to their native form (Weill et al., 2019).

To further explore the mitochondrial targeting role of N25, a construct fusing the N25 segment from MagR to the N-terminus of EGFP was created, with both the N25-EGFP fusion protein and EGFP alone then expressed in HeLa cells. Fluorescence microscopy was used to observe the distribution of EGFP proteins, while the mitochondria were stained with antibodies against Tom20. Results showed that N25-EGFP fusion proteins were predominantly co-localized with Tom20, indicating successful mitochondrial targeting. In contrast, cells expressing EGFP proteins alone exhibited diffuse cellular distribution, lacking specific mitochondrial localization (Figure 1B). The intensity of Tom20 fluorescence remained consistent across all cell groups (Supplementary Figure S1B).

Taken together, the N25 of clMagR appear to function as a mitochondrial targeting signal (MTS), playing an indispensable role in the mitochondrial localization of MagR within cells.

N25 residues are not cleaved during maturation and influence iron-sulfur cluster and iron binding efficiency in clMagR

Typically, mitochondrial matrix protein maturation involves the cleavage of MTS sequences by mitochondrial processing

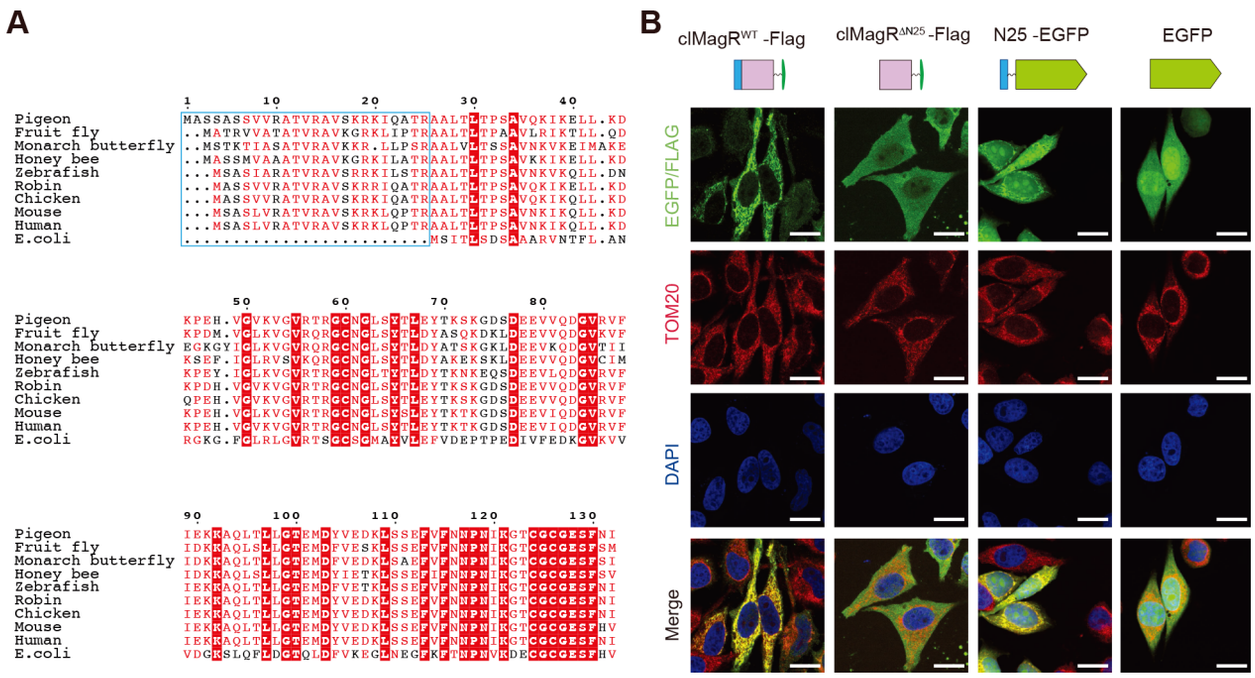

Figure 1 clMagR N-terminal sequence and its function in mitochondrial localization

A: Sequence alignment of MagR from 10 representative prokaryotic and eukaryotic species. Residues with high similarity across species are shown in red and 100% conserved amino acids are shown in white with red background. Less conserved 25 amino acids in the N-terminal region of MagR are shown in the blue box. B: Confocal images of HeLa cells expressing wild-type clMagR fused with Flag-tag (clMagR^{WT}-Flag) or N25-deleted clMagR fused with Flag-tag (clMagR$^{\Delta N25}$-Flag) or N25 fused with EGFP (N25-EGFP) or EGFP. clMagR^{WT}-Flag, clMagR$^{\Delta N25}$-Flag, N25-EGFP, and EGFP shown as green with staining of anti-Flag antibodies or fluorescence of EGFP. Mitochondria were stained with antibodies against Tom20 and are shown in red. Cell nuclei were stained with DAPI (blue). Areas with yellow fluorescence in merged images denote co-localization of proteins within mitochondria. Scale bars represent 20 μm.

peptidase. However, for certain proteins, these MTS sequences are not excised (Bedwell et al., 1989; Bykov et al., 2022; Poveda-Huertes et al., 2020; Zhang et al., 2020). To determine whether the MTS associated with clMagR undergoes cleavage upon mitochondrial entry, wild-type and N25-truncated clMagR fused with Flag-tag (clMagR^{WT}-Flag and clMagR$^{\Delta N25}$-Flag) on the C-terminal were expressed in HeLa cells, with immunoblotting then performed to detect mature clMagR proteins. Notably, immunoblotting revealed a single band at the expected molecular weight for cells transfected with clMagR^{WT}-Flag and clMagR$^{\Delta N25}$-Flag, indicating that the N25 MTS from full-length clMagR^{WT} was not cleaved after mitochondrial entry *in vivo* (Figure 2A).

Considering the significant variability in the N-terminal 25 residue region of MagR sequences across different species, from *E. coli* to eukaryotes, we investigated the specific function of the N25 sequences in mature MagR. Three constructs were designed for wild-type and N25 truncated clMagR and wild-type IscA from *E. coli* fused with a Strep tag at the N-terminus (Figure 2B). These proteins were expressed in *E. coli* cells under aerobic conditions and subsequently purified to homogeneity for analysis. The SEC results revealed eluting peaks with nearly identical retention volumes for all three proteins (Figure 2C). Furthermore, CD spectra within the ultraviolet region (190–260 nm) were collected to assess the secondary structure of the proteins (Figure 2D). The CD spectra and derived structural proportions for both the wild-type and N25-truncated clMagR were similar, consistent with the SEC results, indicating that N25 did not affect the protein assembly status of clMagR.

As a putative magnetoreceptor, one of the most important features of clMagR is its iron-sulfur cluster-binding properties, which plays an essential role in its magnetism (Guo et al., 2021; Qin et al., 2016; Wang et al., 2024; Xie, 2022; Zhou et al., 2023). Interestingly, during the clMagR purification process, the colors of the purified clMagR$^{\Delta N25}$ and IscA proteins were markedly lighter than the dark brown clMagR^{WT} proteins in solution when adjusted to equal concentrations (Figure 3A). UV-Vis absorption spectra were used to further quantify iron-sulfur cluster binding. Both clMagR^{WT} and clMagR$^{\Delta N25}$ showed three major absorption peaks at 315 nm, 415 nm, and a shoulder at 456 nm (Figure 3A), indicating the binding of iron-sulfur clusters in both proteins. However, the absorption of clMagR$^{\Delta N25}$ was much lower than that of clMagR^{WT}, consistent with the appearance of the protein solution, suggesting that the binding efficiency of the iron-sulfur clusters was significantly reduced by the truncation of N25. In addition, unlike wild-type and N25-truncated clMagR, IscA only exhibited one major absorption peak at 315 nm and an extremely low absorption peak at 415 nm, indicating low or no iron-sulfur cluster binding (Figure 3A).

Total iron content of the three proteins was measured using the ferrozine assay, developed to quantify iron content in biological systems. As shown in Figure 3B, iron content was significantly lower in clMagR$^{\Delta N25}$ than in wild-type clMagR and even lower than in IscA, indicating that truncation of N25 impaired total iron content in clMagR, consistent with the coloration and UV-Vis spectra results.

To explore the role of N25 in iron binding in clMagR, iron reconstitution experiments were performed for purified clMagR^{WT} and clMagR$^{\Delta N25}$. The proteins were incubated with a series of concentrations of ferrous iron in the presence of

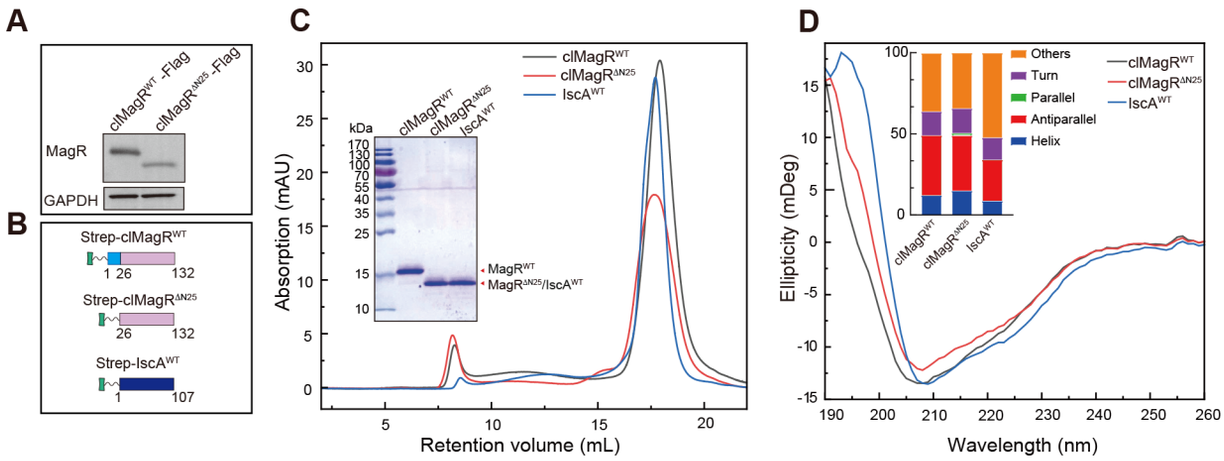

Figure 2 N25 was preserved in mature clMagR and did not affect protein assembly status

A: Cell extracts were analyzed by immunoblotting for indicated clMagR proteins using anti-Flag-tag and anti-GAPDH antibodies. B: Schematic representation of plasmid construction for wild-type and N25-truncated clMagR and *E. coli* IscA with a Strep-tag fused on the N-terminal for expression in *E. coli*. C: Size-exclusion chromatography of wild-type (clMagR^{WT}, black line) and N25-truncated clMagR (clMagR$^{\Delta N25}$, red line) and IscA (blue line) on a Superose 6 Increase 10/300 chromatography column. SDS-PAGE of purified proteins is shown as insert. D: CD spectra of clMagR^{WT}, clMagR$^{\Delta N25}$ and IscA, shown in same color as in (C). Proportion of secondary structures for each protein is shown as insert.

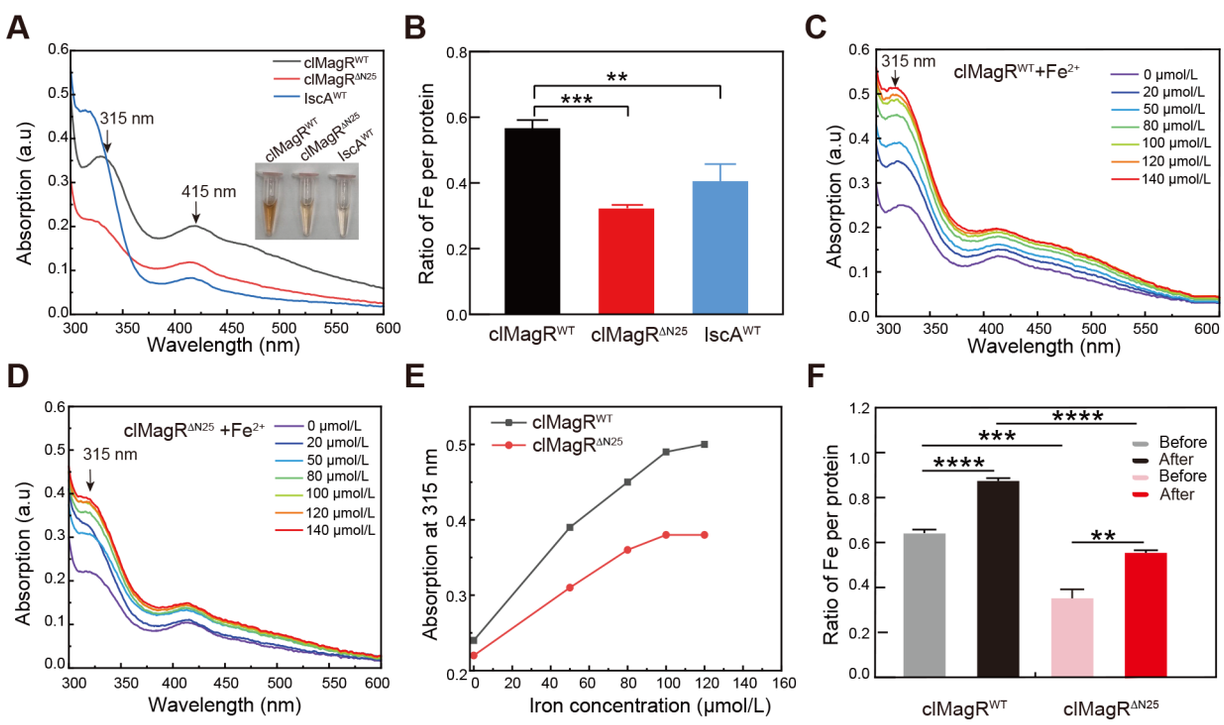

Figure 3 N25 affected iron-sulfur cluster and iron binding in clMagR

A: UV-visible absorption spectra of clMagR^{WT} (black), clMagR$^{\Delta N25}$ (red), and IscA (blue). Insert picture shows protein solution. B: Total iron content of purified clMagR^{WT} (black), clMagR$^{\Delta N25}$ (red), and IscA (blue) measured by ferrozine assay and presented as the ratio of iron atoms in each protein. Student's *t*-test: **: P<0.01; ***: P<0.001. Error bars represent standard error of the mean (SEM) calculated from three independent experiments. C, D: UV-visible absorption spectra of clMagR^{WT} (C) and clMagR$^{\Delta N25}$ (D) after reconstitution with iron. E: Iron binding curves of clMagR^{WT} (black) and clMagR$^{\Delta N25}$ (red). Amplitudes of absorption peak at 315 nm for proteins obtained from spectra in C and D. F: Total iron content of purified clMagR^{WT} and clMagR$^{\Delta N25}$ proteins without and with reconstitution of 120 μmol/L iron measured by ferrozine assay as the ratio of iron atoms per protein monomer. Data are shown as mean±SEM calculated from three independent experiments. Student's *t*-test: **: P<0.01; ****: P<0.0001.

DTT at room temperature, followed by repurification of the proteins using standard procedures, as described previously (Zhou et al., 2023). As shown in Figure 3C, a significant dose-dependent increase in absorption at 315 nm was detected for clMagR^{WT} after iron reconstitution. However, unlike the fast iron loading observed in wild-type clMagR, the UV-Vis absorption peak at 315 nm for clMagR$^{\Delta N25}$ only slightly increased after incubation with ferrous iron (Figure 3D, E). Consistently, total iron content in purified clMagR^{WT} was much higher than that in clMagR$^{\Delta N25}$ after incubation with 120 μmmol/L ferrous iron, as determined by the ferrozine assay (Figure 3F), indicating that iron binding capacity was strongly

affected by truncation of N25.

Previous studies have also shown that clMagR acts as a carrier protein to transfer iron-sulfur clusters from IscU in the presence of L-cysteine, cysteine desulfurase (IscS), and DTT (Blanc et al., 2015; Ding et al., 2005; Zhou et al., 2023). Here, to test whether N25 affects the iron transfer ability of clMagR, wild-type and N25-truncated apo-clMagR were separately incubated with His-tagged IscU for 180 min in the presence of DTT. After reaction and separation, UV-Vis spectra for the IscU and clMagR proteins were recorded. The typical clMagR^{WT} peaks at 315 nm and 415 nm were significantly increased after the reaction (Supplementary Figure S2A), indicating the [2Fe-2S] cluster was transferred from IscU to clMagR^{WT}. The UV-Vis absorption of clMagR$^{\Delta N25}$ was also slightly increased but much lower than that of wild-type clMagR (Supplementary Figure S2B, C). Correspondingly, the UV-Vis absorption of IscU was much lower after incubation with clMagR^{WT} than with clMagR$^{\Delta N25}$ (Supplementary Figure S2D), suggesting that the iron-sulfur clusters transferred from holo-IscU to two clMagR proteins, but transfer efficiency was lower in clMagR$^{\Delta N25}$. Consistently, when iron-loaded clMagR^{WT} and clMagR$^{\Delta N25}$ were incubated with apo-IscU, a huge decrease in UV-Vis absorption was observed for clMagR^{WT} (Supplementary Figure S3A), while only minor changes were observed for clMagR$^{\Delta N25}$ (Supplementary Figure S3B). In addition, compared to the significant absorption increase in IscU after incubation with clMagR^{WT} (Supplementary Figure S3C), IscU only received a small amount of iron from clMagR$^{\Delta N25}$, with a minor increase in UV-Vis absorption after incubation (Supplementary Figure S3D).

Taken together, these findings indicate that the N25 sequences of clMagR are not cleaved during protein maturation and play important roles in both iron-cluster and iron binding in clMagR.

N25 residues did not affect iron-sulfur cluster types in clMagR

Mononuclear ferric iron and iron-sulfur clusters, including [3Fe-4S] and [2Fe-2S], bind to clMagR and distinct magnetic properties (Zhou et al., 2023). To further investigate the impact of N25 on the iron-sulfur cluster types associated with clMagR, EPR spectroscopy was applied to assess the states of wild-type and N25-truncated clMagR proteins.

As shown in Figure 4A, wild-type and N25-truncated clMagR, as well as IscA, displayed a signal at g=4.3, indicating mononuclear ferric iron binding in each protein, as reported previously (Zhou et al., 2023). This suggests that N25 truncation did not affect mononuclear ferric iron binding in clMagR. CD spectroscopy was then applied to analyze the types of iron-sulfur clusters and their protein environments. All three proteins showed two positive peaks at 371 nm and 426 nm and two negative peaks at 396 nm and 463 nm (Figure 4B), suggesting the binding of the [2Fe-2S] cluster (Azam et al., 2020) in the three proteins, consistent with previous studies (Guo et al., 2021; Tong et al., 2022b).

While [2Fe-2S] shows typical absorbance in CD spectroscopy, the [4Fe-4S] and [3Fe-4S] clusters usually exhibit negligible CD intensity, complicating their detection via CD methods. Therefore, EPR was used to determine the possible existence of [4Fe-4S] and [3Fe-4S] in the clMagR and IscA proteins. Both the oxidized and reduced states of clMagR^{WT}, clMagR$^{\Delta N25}$, and IscA were measured by EPR. As shown in Figure 4C, oxidized clMagR^{WT} was characterized by a rhombic EPR signal with typical g values at g_1=2.01, g_2=2.00, and g_3=1.99, which disappeared when temperatures reached 45 K, indicative of [3Fe-4S] binding (Beilschmidt et al., 2017; Liu et al., 2013). Upon reduction with sodium dithionite, signals corresponding to the [2Fe-2S] cluster were observed at 45 K and 60 K (Figure 4D), consistent with prior findings (Guo et al., 2021; Thompson et al., 2022; Tong et al., 2022b). Similar EPR signals were observed for both N25-truncated clMagR (Figure 4E, F) and IscA (Figure 4G, H) in their oxidized and reduced states compared to wild-type clMagR, indicating that the binding of iron-sulfur clusters is not affected by the N-terminal 25 residues of clMagR.

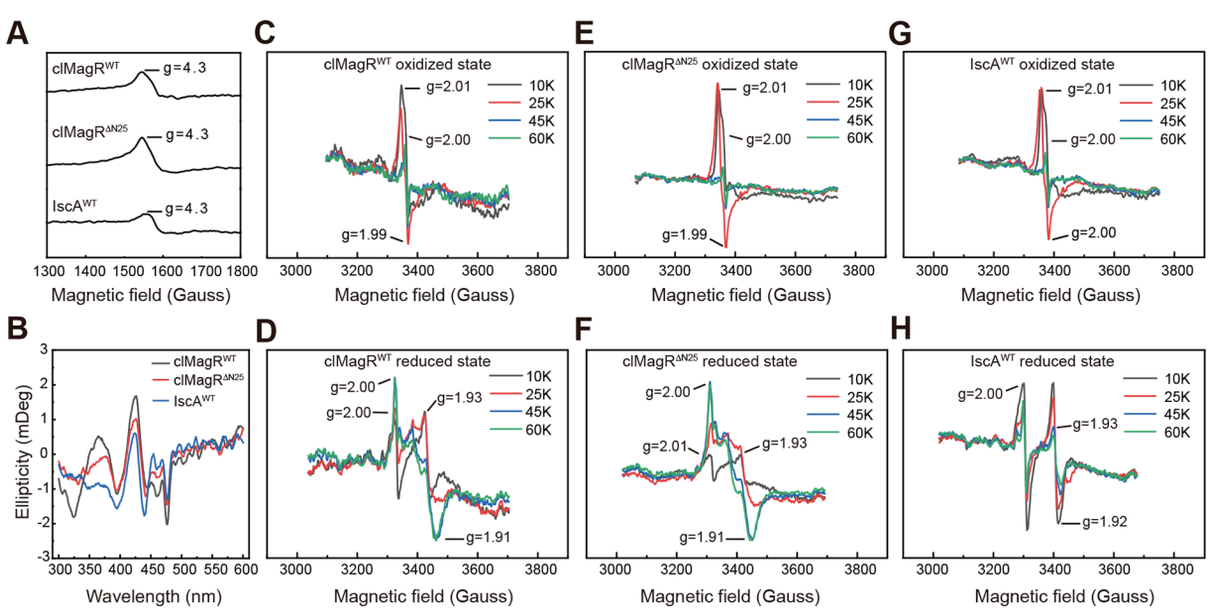

Figure 4 N25 did not affect iron-sulfur cluster types in clMagR

A: EPR spectra of clMagR^{WT}, clMagR$^{\Delta N25}$, and IscA recorded at 10 K. B: CD spectra of purified clMagR^{WT} (black line), clMagR$^{\Delta N25}$ (red line), and IscA (blue line). C–H: X-band EPR spectra of as-purified clMagR^{WT} (C, D), clMagR$^{\Delta N25}$ (E, F), and IscA (G, H). EPR experiments were performed both at oxidized (upper) and reduced states (bottom), and recorded at different temperatures (10 K, 25 K, 45 K, and 60 K).

N25 residues involved in MagR/Cry complex formation

In addition to its iron sulfur binding capacity, MagR is recognized for its ability to form a rod-like complex with Cry, which functions in magnetic field sensing as a biological compass. While N-terminal motif 6 of MagR is implicated in the interaction with Cry based on structural simulation (Lu et al., 2020), experimental evidence is lacking. Thus, to determine whether the N-terminal 25 residues of clMagR play a role in complex formation with Cry, several constructs were designed with a Strep tag fused to the N-terminal of wild-type and N25-truncated clMagR and a His tag fused to the N-terminal of Cry. Co-expression of Strep-tagged wild-type and N25-truncated clMagR with His-tagged Cry led to the identification and purification of the protein complexes using a two-step tandem affinity purification procedure (Figure 5A). Results showed stable interactions between clMagR^{WT} and Cry, evident from two clear bands corresponding to their molecular weights on SDS-PAGE post-purification (Figure 5B). However, the purification of the clMagR$^{\Delta N25}$ and clCry4 complex yielded a clear band for clCry with a smear and much weaker band for clMagR$^{\Delta N25}$ (Figure 5B), indicating truncation of N25 strongly impairs clMagR$^{\Delta N25}$/clCry4 complex formation. These findings are consistent with the assumption that the N-terminal motif of MagR plays an essential role in magnetic compass formation (Lu et al., 2020; Xie, 2022).

DISCUSSION

MagR/IscA1 in eukaryotes and its prokaryotic homolog IscA are widely distributed across all major phyla, with the major distinction being the presence of 20–30 N-terminal amino acids in MagR/IscA1, which are absent in IscA. In eukaryotes, MagR/IscA1 is primarily located in mitochondria and involved in various biological processes, including the biogenesis and assembly of iron-sulfur clusters (Cózar-Castellano et al., 2004). MagR has also recently been identified as a putative magnetoreceptor, forming a rod-like complex with Cry that serves as a biological compass for magnetoreception (Qin et al., 2016), with potential involvement of electron-transfer reactions (Xie, 2022). Despite the high conservation of C-terminal sequences of MagR in different species, N-terminal sequences exhibit considerable divergence across species, especially between eukaryotes and prokaryotes. However, whether the N-terminal sequences play a specific role in MagR functions remains unknown. Notably, our study confirmed the N-terminal 25 residues of clMagR serve as a signal peptide for mitochondrial localization, aligning with the general mitochondrial localization observed for MagR proteins. Surprisingly, the N25 sequences were not cleaved following protein maturation, yet this did not influence the overall assembly of MagR in comparison to IscA in bacteria. The absence of N-terminal residues in IscA did not alter the protein assembly between MagR and IscA across various species, suggesting a shared functional role in iron metabolism.

Interestingly, N25 strongly affected the binding efficiency but not the types of iron-sulfur clusters and iron in clMagR (Figure 3). This observation is consistent with previous research showing that iron binding is mediated with the conserved Y65 residue, while iron-sulfur cluster binding is mediated by three conserved cysteines, C60, C124, and C126, located in the central and C-terminal regions of MagR, distinct from the N25 region (Tong et al., 2022b; Zhou et al., 2023). Thus, truncation of N25 did not directly impact the binding of iron-sulfur clusters (Figure 4), nor the assembly status of clMagR (Figure 2). Therefore, our findings suggest a possible allosteric regulation mechanism by which N25 influence iron and iron-sulfur cluster binding, warranting further investigation. Additionally, N25 may mediate protein-protein interactions between MagR and other iron-sulfur assembly proteins, as well as Cry proteins. In support of this, recent research has shown unexpected divergence in MagR between robins and pigeons, attributed to two sequence variations in the N-terminal region (Wang et al., 2024).

Our results also demonstrated the critical role of the N25 in MagR and Cry complex formation, with significant impairment in their interaction upon N25 truncation. This observation is in agreement with the previous assumption suggesting that the N-terminal motif of MagR may be located at the interface between tetramers, potentially impacting magnetic compass assembly, as deduced from structural simulations (Qin et al., 2016; Yang et al., 2022). However, detailed protein structure analysis has so far been limited to bacterial IscA, which lacks the N-terminal 25 residues present in eukaryotic MagR, leaving a gap in structural information for this specific N-terminal region. Overall, this study highlights the importance of the MagR N-terminal region in MagR and Cry complex formation and provides potential guidance for future structural studies on the MagR/Cry biocompass.

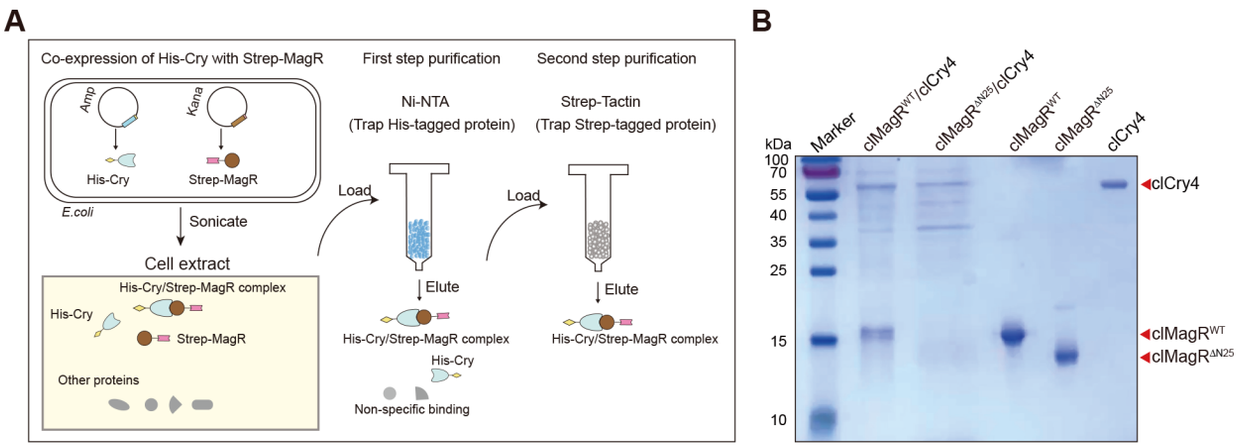

Figure 5 Tandem affinity purification of clMagR/clCry complex

A: Schematic showing co-expression and co-purification of clMagR/clCry complex based on interactions between cryptochrome (cyan) and MagR (brown). B: SDS-PAGE of purified clMagR, clCry4, and clMagR/clCry complexes. clMagR^{WT}, clMagR$^{\Delta N25}$, and clCry are indicated with arrows.

Viewed through an evolutionary lens, iron metabolism represents a universal necessity for life, whereas magnetoreception is an adaptive trait evolved by some species to enhance their navigational and migratory capabilities. Regions of proteins that are less conserved represent sites of slow evolution, which may not directly alter protein function but can significantly impact protein characteristics. This concept is supported by recent findings reporting the biochemical and biophysical divergence in MagR between robins and pigeons, attributed to two sequence variations in the N-terminal region (Wang et al., 2024). In the current study, the additional N-terminal 25 residues of clMagR, absent in bacterial IscA, enhanced assembly efficiency of iron-sulfur in eukaryotes and introduced a novel function for interaction with Cry in magnetoreception. Given the variability of the N-terminal sequences of MagR among different species, the N-terminal 25 residues identified here may serve as a footprint for understanding how magnetoreception evolved in animals over time.

From an evolutionary viewpoint, less conserved regions of proteins that evolved slowly may not directly alter the primary function of a protein, but can profoundly affect protein conformation, stability, and the specificity of its interactions with other proteins. In the context of MagR, the N25 segment showed less evolutionary conservation compared to other segments of MagR, and while it did not change the types of iron and iron-sulfur clusters that MagR binds to, it did influence the efficiency of these bindings and the formation of complexes with Cry. This suggests that the N25 segment may affect the unique interaction dynamics between MagR and Cry in various species, presenting an intriguing area for future research.

Collectively, our study revealed that the N-terminal 25 residues of clMagR extend beyond merely serving as a MTS. They also significantly enhance the binding efficiency of both iron-sulfur clusters and iron in eukaryotic MagR proteins compared to prokaryotic IscA and mediate the interaction between MagR and Cry for the formation of a putative magnetic biocompass. These discoveries advance our understanding of the diversity and molecular mechanisms of animal navigation from an evolutionary perspective and provide insights into the future design of MagR as a potential molecular magnetic tool via modulation of this N-terminal region.

SUPPLEMENTARY DATA

Supplementary data to this article can be found online.

COMPETING INTERESTS

The authors declare that they have no competing interests.

AUTHORS' CONTRIBUTIONS

T.C. and C.X. conceived the idea and designed the study. Y.Z. carried out protein purification, ferrozine assay, CD spectroscopy, UV-vis measurements, EPR experiments, and western blotting. Y.Z. and T.C. performed data analysis. T.T. and Y.Z. helped with *in vitro* iron-sulfur and iron transfer experiments. J.W., C.F., and J.Z. provided valuable suggestions on immunofluorescence staining. P.Z. and X.Z. contributed to the construction of recombinant plasmids. X.Z., J.L., and M.W. provided valuable discussions and edited the manuscript. Y.Z., T.C., and C.X. wrote the paper. All authors read and approved the final version of the manuscript.

ACKNOWLEDGMENTS

We are grateful to the core facilities of the College of Life Sciences at the University of Science and Technology of China and the College of Life Sciences of Anhui University for their help in CD spectral measurements. We thank the Steady High Magnetic Field Facilities (High Magnetic Field Laboratory, CAS) for assistance with EPR measurements, and thank Dr. Wei Tong and Jinxing Li for their technical support. We also thank Xinmiao Ji for assistance in confocal microscopy observations and Huangtao Xu for very helpful discussions.

REFERENCES

Arai S, Shimizu R, Adachi M, et al. 2022. Magnetic field effects on the structure and molecular behavior of pigeon iron–sulfur protein. Protein Science, 31(6): e4313.

Arai S, Shimizu R, Adachi M, et al. 2023. Novel function of pigeon iron–sulfur protein for the magnetoreception predicted by SAXS analysis with a permanent magnetic device. Photon Factory Activity Report.

Azam T, Przybyla-Toscano J, Vignols F, et al. 2020. The arabidopsis mitochondrial glutaredoxin GRXS15 provides [2Fe-2S] clusters for ISCA-mediated [4Fe-4S] cluster maturation. International Journal of Molecular Sciences, 21(23): 9237.

Bedwell DM, Strobel SA, Yun K, et al. 1989. Sequence and structural requirements of a mitochondrial protein import signal defined by saturation cassette mutagenesis. Molecular and Cellular Biology, 9(3): 1014–1025.

Beilschmidt LK, de Choudens SO, Fournier M, et al. 2017. ISCA1 is essential for mitochondrial Fe_4S_4 biogenesis *in vivo*. *Nature Communications*, **8**: 15124.

Blanc B, Gerez C, de Choudens SO. 2015. Assembly of Fe/S proteins in bacterial systems: biochemistry of the bacterial ISC system. Biochimica et Biophysica Acta (BBA) - Molecular Cell Research, 1853(6): 1436–1447.

Bykov YS, Flohr T, Boos F, et al. 2022. Widespread use of unconventional targeting signals in mitochondrial ribosome proteins. The EMBO Journal, 41(1): e109519.

Chang H, Fu XW, Zhao SY, et al. 2017. Molecular characterization, tissue, and developmental expression profiles of *MagR* and *Cryptochrome* genes in *Agrotis ipsilon* (lepidoptera: noctuidae). Annals of the Entomological Society of America, 110(4): 422–432.

Chang H, Guo JL, Fu XW, et al. 2018. Molecular characterization and expression profiles of *IscA1* gene in a long-distance migrant. Agrotis segetum. Journal of Asia-Pacific Entomology, 21(4): 1299–1306.

Cózar-Castellano I, del Valle Machargo M, Trujillo E, et al. 2004. hIscA: a protein implicated in the biogenesis of iron-sulfur clusters. *Biochimica et Biophysica Acta* (*BBA*) - *Proteins and Proteomics*, **1700**(2): 179–188.

Ding HG, Harrison K, Lu JX. 2005. Thioredoxin reductase system mediates iron binding in IscA and iron delivery for the iron-sulfur cluster assembly in IscU. Journal of Biological Chemistry, 280(34): 30432–30437.

Eder SHK, Cadiou H, Muhamad A, et al. 2012. Magnetic characterization of isolated candidate vertebrate magnetoreceptor cells. Proceedings of the National Academy of Sciences of the United States of America, 109(30): 12022–12027.

Garcia PS, D'Angelo F, de Choudens SO, et al. 2022. An early origin of iron-sulfur cluster biosynthesis machineries before Earth oxygenation. Nature Ecology & Evolution, 6(10): 1564–1572.

Gegear RJ, Casselman A, Waddell S, et al. 2008. Cryptochrome mediates light-dependent magnetosensitivity in *Drosophila*. *Nature*, **454**(7207): 1014–1018.

Guo Z, Xu S, Chen X, et al. 2021. Modulation of MagR magnetic properties via iron–sulfur cluster binding. Scientific Reports, 11(1): 23941.

Hjort K, Goldberg AV, Tsaousis AD, et al. 2010. Diversity and reductive evolution of mitochondria among microbial eukaryotes. Philosophical Transactions of the Royal Society B:Biological Sciences, 365(1541):

713–727.

Hore PJ, Mouritsen H. 2016. The radical-pair mechanism of magnetoreception. Annual Review of Biophysics, 45: 299–344.

Hsu CY, Chan YP. 2011. Identification and localization of proteins associated with biomineralization in the iron deposition vesicles of honeybees (*Apis mellifera*). PLoS One, 6(4): e19088.

Im J, Lee J, Löffler FE. 2013. Interference of ferric ions with ferrous iron quantification using the ferrozine assay. Journal of Microbiological Methods, 95(3): 366–367.

Jin MH, Liu B, Zheng WG, et al. 2023. Chromosome-level genome of black cutworm provides novel insights into polyphagy and seasonal migration in insects. BMC Biology, 21(1): 2.

Lill R, Diekert K, Kaut A, et al. 1999. The essential role of mitochondria in the biogenesis of cellular iron-sulfur proteins. Biological Chemistry, 380(10): 1157–1166.

Liu YD, Guo SH, Yu RL, et al. 2013. HdrC2 from *Acidithiobacillus ferrooxidans* owns two iron–sulfur binding motifs but binds only one variable cluster between [4Fe–4S] and [3Fe–4S]. Current Microbiology, 66(1): 88–95.

Lu HM, Li JD, Zhang YD, et al. 2020. The evolution history of Fe-S cluster A-type assembly protein reveals multiple gene duplication events and essential protein motifs. Genome Biology and Evolution, 12(3): 160–173.

Mannino G, Casacci LP, Bianco Dolino G, et al. 2023. The geomagnetic field (GMF) is necessary for black garden ant (*Lasius niger* L.) foraging and modulates orientation potentially through aminergic regulation and *MagR* expression. International Journal of Molecular Sciences, 24(5): 4387.

Monteil CL, Lefevre CT. 2020. Magnetoreception in microorganisms. Trends in Microbiology, 28(4): 266–275.

Ollagnier-de Choudens S, Nachin L, Sanakis Y, et al. 2003. SufA from *Erwinia chrysanthemi*: characterization of a scaffold protein required for iron-sulfur cluster assembly. Journal of Biological Chemistry, 278(20): 17993–18001.

Poveda-Huertes D, Matic S, Marada A, et al. 2020. An early mtUPR: redistribution of the nuclear transcription factor rox1 to mitochondria protects against intramitochondrial proteotoxic aggregates. *Molecular Cell*, **77**(1): 180–188. e9.

Qin SY, Yin H, Yang CL, et al. 2016. A magnetic protein biocompass. Nature Materials, 15(2): 217–226.

Schulten K, Wolynes PG. 1978. Semiclassical description of electron spin motion in radicals including the effect of electron hopping. The Journal of Chemical Physics, 68(7): 3292–3297.

Song DS, Tu Z, Lee FS. 2009. Human ISCA1 interacts with IOP1/NARFL and functions in both cytosolic and mitochondrial iron-sulfur protein biogenesis. Journal of Biological Chemistry, 284(51): 35297–35307.

Thompson Z, Fidai I, Wachnowsky C, et al. 2022. Spectroscopic and functional characterization of the [2Fe–2S] scaffold protein Nfu from *Synechocystis* PCC6803. Biochimie, 192: 51–62.

Tong DD, Zhang L, Wu NN, et al. 2022a. The oriental armyworm genome yields insights into the long-distance migration of noctuid moths. Cell Reports, 41(12): 111843.

Tong TY, Zhou YJ, Fei F, et al. 2022b. The rational design of iron-sulfur cluster binding site for prolonged stability in magnetoreceptor MagR. Frontiers in Molecular Biosciences, 9: 1051943.

Tsaousis AD. 2019. On the origin of iron/sulfur cluster biosynthesis in eukaryotes. Frontiers in Microbiology, 10: 2478.

Walcott C, Gould JL, Kirschvink J. 1979. Pigeons have magnets. Science, 205(4410): 1027–1029.

Wang S, Zhang P, Fei F, et al. 2024. Unexpected divergence in magnetoreceptor MagR from robin and pigeon linked to two sequence variations. Zoological Research, 45(1): 69–78.

Weill U, Krieger G, Avihou Z, et al. 2019. Assessment of GFP tag position on protein localization and growth fitness in yeast. Journal of Molecular Biology, 431(3): 636–641.

Xie C. 2022. Searching for unity in diversity of animal magnetoreception: from biology to quantum mechanics and back. The Innovation, 3(3): 100229.

Xu JJ, Jarocha LE, Zollitsch T, et al. 2021. Magnetic sensitivity of cryptochrome 4 from a migratory songbird. Nature, 594(7864): 535–540.

Yang PL, Cai TT, Zhang L, et al. 2022. A rationally designed building block of the putative magnetoreceptor MagR. Bioelectromagnetics, 43(5): 317–326.

Zhang S, Reljić B, Liang C, et al. 2020. Mitochondrial peptide BRAWNIN is essential for vertebrate respiratory complex III assembly. Nature Communications, 11(1): 1312.

Zhou YJ, Tong TY, Wei MK, et al. 2023. Towards magnetism in pigeon MagR: iron- and iron-sulfur binding work indispensably and synergistically. Zoological Research, 44(1): 142–152.